NATIONAL ADVISORY COMMITTEE FOR AERONAUTICS

REPORT 1281

FLIGHT DETERMINATION OF DRAG OF NORMAL-SHOCK NOSE INLETS WITH VARIOUS COWLING PROFILES AT MACH NUMBERS FROM 0.9 TO 1.5

By R. I. SEARS, C. F. MERLET, and L. W. PUTLAND

1956

For sale by the Superintendent of Documents, U. S. Government Printing Office, Washington 25, D. C. Yearly subscription, $10; foreign, $11.25; single copy price varies according to size - - - - - - - - - Price 25 cents

REPORT 1281

FLIGHT DETERMINATION OF DRAG OF NORMAL-SHOCK NOSE INLETS WITH VARIOUS COWLING PROFILES AT MACH NUMBERS FROM 0.9 TO 1.5

By R. I. SEARS, C. F. MERLET, and L. W. PUTLAND

Langley Aeronautical Laboratory

Langley Field, Va.

National Advisory Committee for Aeronautics

Headquarters, 1512 H Street NW., Washington 25, D. C.

Created by act of Congress approved March 3, 1915, for the supervision and direction of the scientific study of the problems of flight (U. S. Code, title 50, sec. 151). Its membership was increased from 12 to 15 by act approved March 2, 1929, and to 17 by act approved May 25, 1948. The members are appointed by the President, and serve as such without compensation.

REPORT 1281

FLIGHT DETERMINATION OF DRAG OF NORMAL-SHOCK NOSE INLETS WITH VARIOUS COWLING PROFILES AT MACH NUMBERS FROM 0.9 TO 1.5 [1]

By R. I. Sears, C. F. Merlet, and L. W. Putland

SUMMARY

Free-flight tests were made with normal-shock nose-inlet models with NACA 1-series, parabolic, and conic cowling profiles to investigate the external drag characteristics at an angle of attack of 0°. The Mach number range of the tests was from 0.9 to 1.5, the mass-flow ratio was from 0.7 to 1.0, and the Reynolds number based on body maximum diameter varied from 2.5×10^6 to 5.5×10^6. Two related nonducted bodies were also tested for comparison purposes.

At the maximum flow rate the inlet models had about the same external drag at a Mach number of approximately 1.1 but at higher Mach numbers the conic cowling had the least drag. Blunting or beveling the lip of the conic cowling while keeping the fineness ratio constant resulted in a slightly higher drag than for the sharp-lip conic cowling at maximum flow rate, but at a mass-flow rate of 0.8 the blunt-, beveled-, and sharp-lip conic cowlings and the parabolic cowling all had about the same drag. The higher drag of the NACA 1–49–300 cowling compared with the blunt-lip conic cowling is associated with the greater fullness back of the inlet.

INTRODUCTION

Because the total-pressure recoveries attainable with normal-shock nose inlets at Mach numbers up to about 1.4 are as good as, or better than, those for other types of inlets, normal-shock inlets are of real interest for aircraft at low supersonic speeds. The Pilotless Aircraft Research Division of the Langley Laboratory has therefore undertaken a program to investigate the drag characteristics of normal-shock nose inlets of various nose geometry. The first phase of this program is concerned with the effects of nose profile and the results are reported herein. A flight technique, differing from that previously used for ducted models, was developed in order to obtain a little information from each of many models rather than more extensive information about only a few models.

Two related nonducted bodies were tested for purposes of comparison with the normal-shock nose-inlet data. Although the models of the present investigation are all nose-inlet models, it is expected that many of the results might also be applicable in the design of scoop inlets.

SYMBOLS

A area, sq ft

A_{cr} critical area (area at which sonic velocity will be obtained, assuming one-dimensional isentropic process), sq ft

C_D drag coefficient, $\dfrac{D}{\frac{1}{2}\rho_\infty V_\infty^2 A_F}$

C_p pressure coefficient, $\dfrac{p-p_\infty}{\frac{1}{2}\rho_\infty V_\infty^2}$

D drag, lb

g acceleration of gravity, 32.2 ft/sec^2

M Mach number

m/m_∞ ratio of mass flow of air through the duct to mass flow of air through a free-stream tube of area equal to inlet area

p static pressure, lb/sq ft

p_t total pressure, lb/sq ft

p_t' pitot stagnation pressure, lb/sq ft

R Reynolds number, based on 7.00-inch body diameter

r radius, in.

t time, sec

V velocity, fps

W weight of the model, lb

x longitudinal distance, measured from the maximum-diameter station, positive downstream, in.

γ ratio of specific heats, 1.40 for air

ρ air density, slugs/cu ft

θ flight-path angle, deg

Subscripts:

∞ free stream

1 first minimum-area station

e exit

ext external

F frontal

i inlet, at lip leading edge

int internal

t total

[1] Supersedes recently declassified NACA Research Memorandum L53I25a by R. I. Sears, C. F. Merlet, and L. W. Putland, 1953.

MODELS

Ducted-nose-inlet models having six different cowling shapes were tested as part of the investigation reported herein. Three models of each cowling shape were tested; each model had a different flow rate. The only difference in the external geometry of the three models for each cowling shape was a slight difference in length, the afterbody being cut off at the station required to give the desired exit area.

Five of the cowlings were of fineness ratio 3 and had an inlet area 24 percent of the body frontal area. The sixth cowling was of fineness ratio 2.5 and had an inlet area 16 percent of the body frontal area. Two related nonducted bodies of revolution were tested—one for each cowling fineness ratio investigated.

The general arrangement of the three model configurations tested for a typical cowling of fineness ratio 3.0 and the related nonducted body is shown in figure 1. Similar information is presented in figure 2 for the cowling models of fineness ratio 2.5. All models had identical fins and afterbody lines.

The afterbody, defined by a parabolic arc with its vertex at the maximum-diameter station, is similar to that used in the inlet investigation reported in reference 1. The coordinates are listed in table I. All afterbodies were spun on the same die from 0.09-inch magnesium and finished to a smooth fair contour and formed the afterportion of the duct. The length at which the afterbody was cut off for each flow rate is shown in figures 1 and 2.

Each model was stabilized by four 60° delta fins having a total exposed area 3.2 times the body frontal area. The airfoil section was hexagonal and was fabricated from ⅛-inch magnesium sheet by beveling the leading and trailing edges.

The nonducted models shown in figures 1 and 2 were related to the ducted models in that coordinates of the duct lips were also coordinates of the nonducted bodies. Thus, the nonducted forebody was defined by a parabolic arc with its vertex at the maximum diameter and passing through the inlet lip. Coordinates are listed in table I.

Details of the various cowling shapes tested are shown in figure 3, and coordinates are given in table I. The external profiles shall be designated by Roman numerals, whereas the internal configurations shall be referred to by Arabic numbers. Cowling I had the NACA 1–49–300 profile (ref. 2). Cowling II had a parabolic profile which was obtained by cutting off at the inlet station the nose of the nonducted body A shown at the top of figure 1. The external lip angle was 9.8°. Cowlings III, IV, and V are called conic because all of cowling III and the major part of the contour of cowlings IV and V were defined by a truncated cone. The cone half-angle was 4.9° for cowling III and 4.4° for cowlings IV and V. Cowling III had sharp lips with an external lip angle of 4.9°. Cowling IV had a beveled lip of external angle 9.8°; the contour in the region of the lips was identical with that of the parabolic cowling II. Cowling V had blunt lips with an external lip angle of 90°. The contour in the region of the lips was identical with that of cowling I of the NACA 1-series. Cowling VI had the NACA 1–40–250 profile.

The external profiles in the region of the lips of the five cowlings of fineness ratio 3.0 are better compared in figure 4.

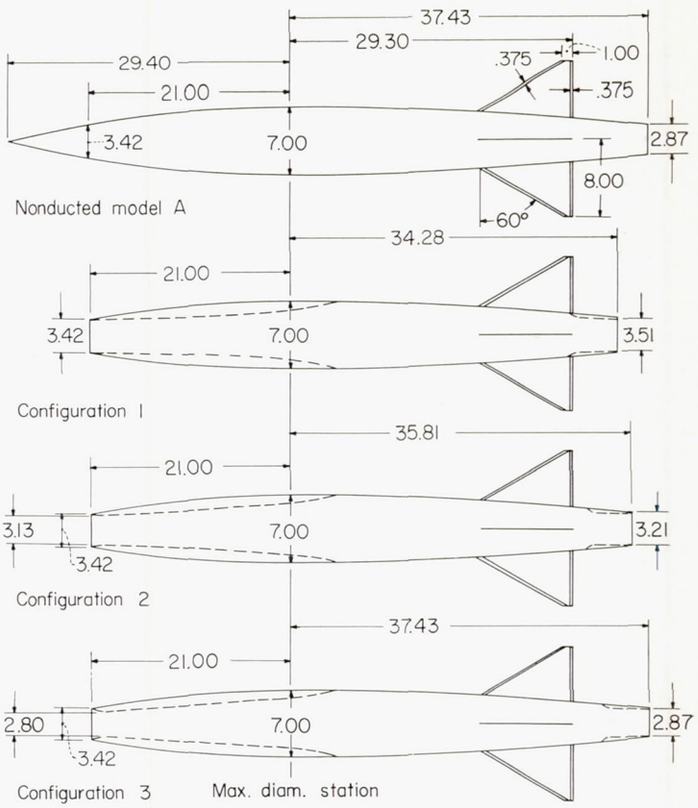

FIGURE 1.—General arrangement of ducted models with cowlings of fineness ratio 3.0 and related nonducted model. All dimensions are in inches.

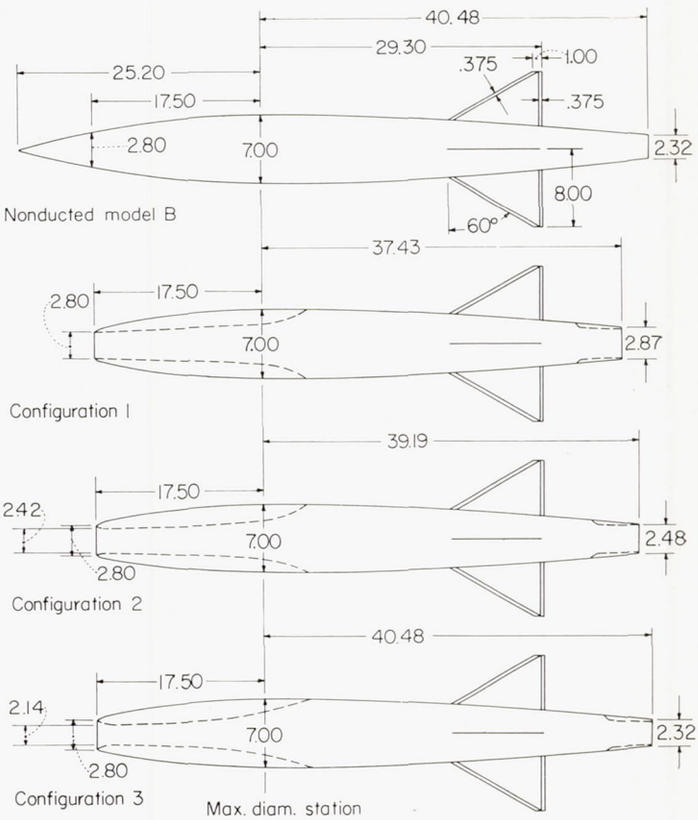

FIGURE 2.—General arrangement of ducted models with cowlings of fineness ratio 2.5 and related nonducted model. All dimensions are in inches.

TABLE I.—EXTERNAL COORDINATES

Nonducted model (from maximum diameter)

Model A forebody	
x, in.	r, in.
−29. 40	0
−28. 90	. 12
−28. 40	. 23
−28. 00	. 33
−27. 00	. 55
−25. 00	. 97
−20. 00	1. 88
−15. 00	2. 59
−10. 00	3. 10
−5. 00	3. 40
0	3. 50

Model B forebody	
x, in.	r, in.
−25. 20	0
−24. 20	. 27
−23. 20	. 53
−22. 20	. 78
−21. 20	1. 02
−20. 20	1. 25
−18. 20	1. 67
−15. 20	2. 23
−10. 20	2. 93
−5. 20	3. 35
0	3. 50

Afterbody	
x, in.	r, in.
0	3. 50
5. 60	3. 45
10. 27	3. 34
15. 87	3. 14
21. 47	2. 84
24. 27	2. 65
30. 80	2. 15
35. 70	1. 68
42. 70	. 90

Normal-shock nose-inlet models—forebody (from maximum diameter)

Cowling I	
x, in.	r, in.
−21. 00	1. 71
−20. 79	1. 90
−20. 37	2. 04
−19. 95	2. 15
−17. 85	2. 52
−14. 70	2. 87
−10. 50	3. 19
−6. 30	3. 39
0	3. 50

Cowling II	
x, in.	r, in.
−21. 00	1. 71
−20. 00	1. 88
−19. 00	2. 04
−18. 00	2. 19
−17. 00	2. 33
−15. 00	2. 59
−10. 00	3. 10
−5. 00	3. 40
0	3. 50

Cowling III	
x, in.	r, in.
−21. 00	1. 71
−10. 00	2. 65
0	3. 50

Cowling IV	
x, in.	r, in.
−21. 00	1. 71
−20. 00	1. 88
−19. 00	2. 04
0	3. 50

Cowling V	
x, in.	r, in.
−21. 00	1. 71
−20. 92	1. 83
−20. 79	1. 90
0	3. 50

Cowling VI	
x, in.	r, in.
−17. 50	1. 40
−17. 40	1. 57
−17. 24	1. 67
−17. 06	1. 75
−16. 63	1. 91
−14. 88	2. 35
−10. 50	2. 97
−5. 25	3. 37
0	3. 50

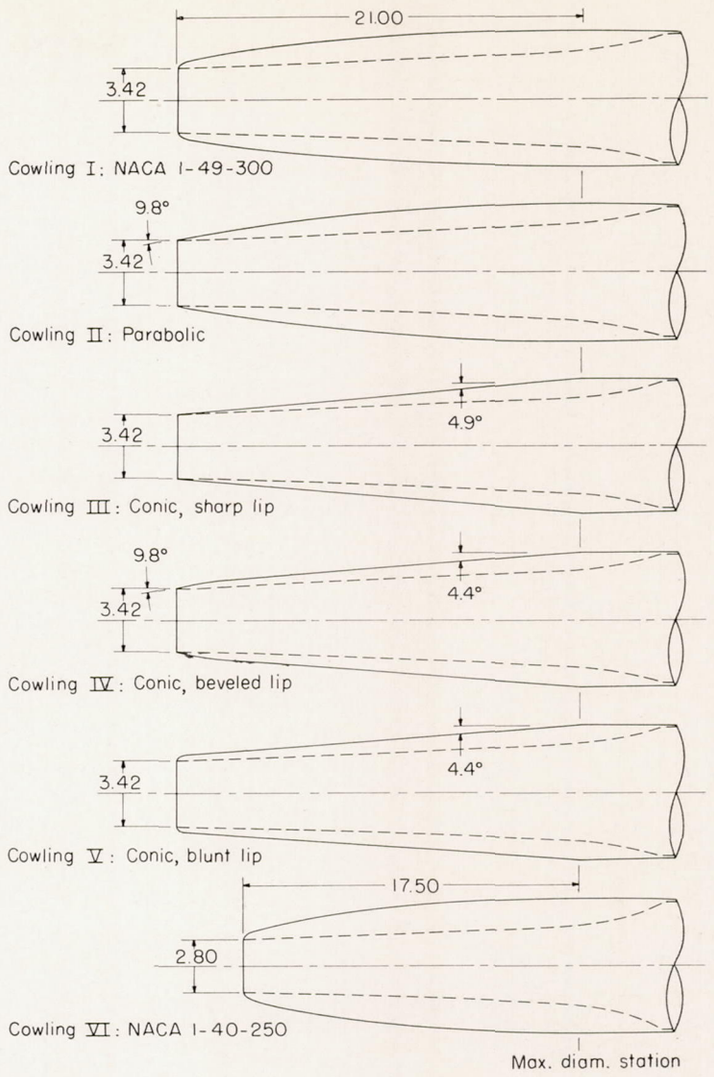

FIGURE 3.—Details of cowling shapes. All dimensions are in inches.

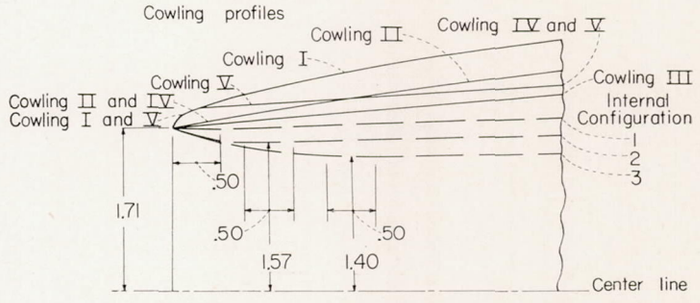

FIGURE 4.—Details of lip shapes of cowlings of fineness ratio 3. All dimensions are in inches.

The three arrangements of internal lines in the region of the inlet designated by the configuration numbers 1, 2, and 3 and used with each cowling shape to regulate the internal air flow are also shown in figure 4. For each cowling shape the internal contraction ratios used were 1.00, 0.83, and 0.67 for configurations 1, 2, and 3, respectively. A similar arrangement, using contraction ratios of 1.00, 0.75, and 0.56, was used for cowling VI which had a smaller inlet area. The minimum section of all models was a cylindrical section ½-inch long, and the internal lips of the models with a contraction ratio less than 1.00 were parabolic from the lip to the minimum section. No attempt was made to measure total-pressure recovery. Details of the diffuser shape are not considered pertinent to this drag investigation and are not presented.

Photographs of the models showing each cowling shape and nonducted body tested are given in figure 5, and the major physical characteristics of the models are presented in table II.

TESTS AND TECHNIQUES

Three models were flown for each normal-shock inlet-cowling shape in order to obtain the variation of C_D with m/m_∞. Different rocket motors were used during the course of the investigation; this fact largely accounts for the different maximum Mach numbers to which data were obtained for the various models. The range of variation of Reynolds number with Mach number is shown in figure 6 for the models tested. All models were flown on a zero-lift trajectory and the data presented are for an angle of attack of 0°.

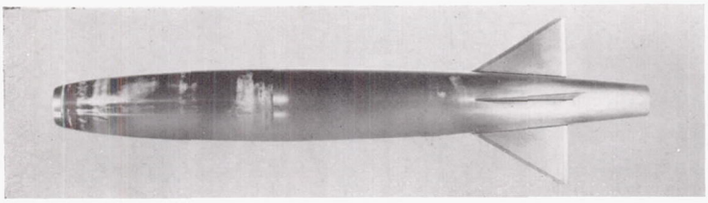

Cowling I: NACA 1–49–300 L–72410.1

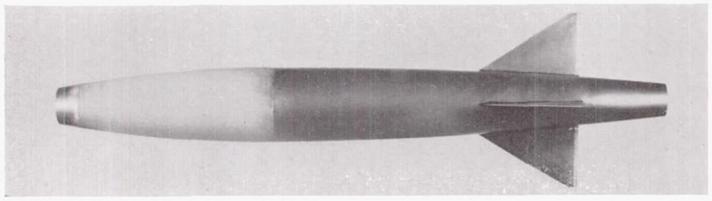

Cowling II: Parabolic L–71587.1

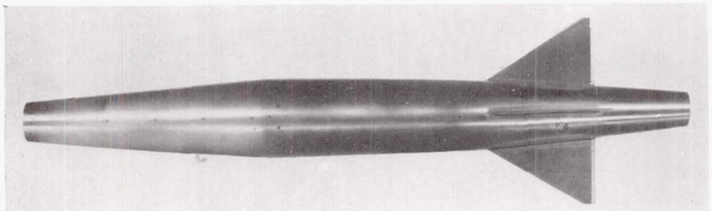

Cowling III: Conic, sharp lip L–73586.1

(a) General views of ducted models.

FIGURE 5.—Photographs of models.

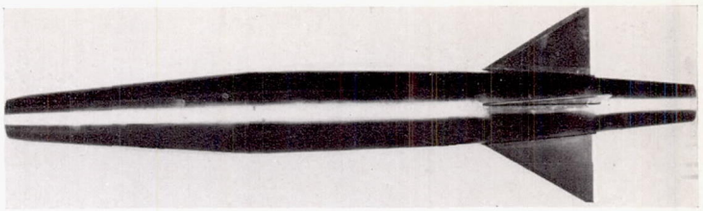

Cowling IV: Conic, beveled lip L–73636.1

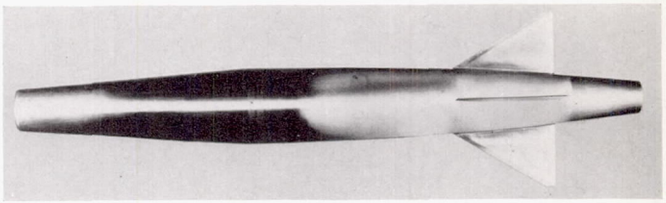

Cowling V: Conic, blunt lip L–75517.1

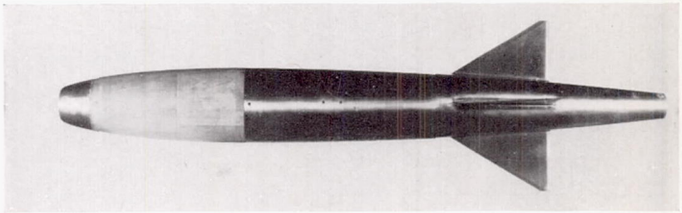

Cowling VI: NACA 1–40–250 L–75361.1

(a) Concluded.

FIGURE 5.—Continued.

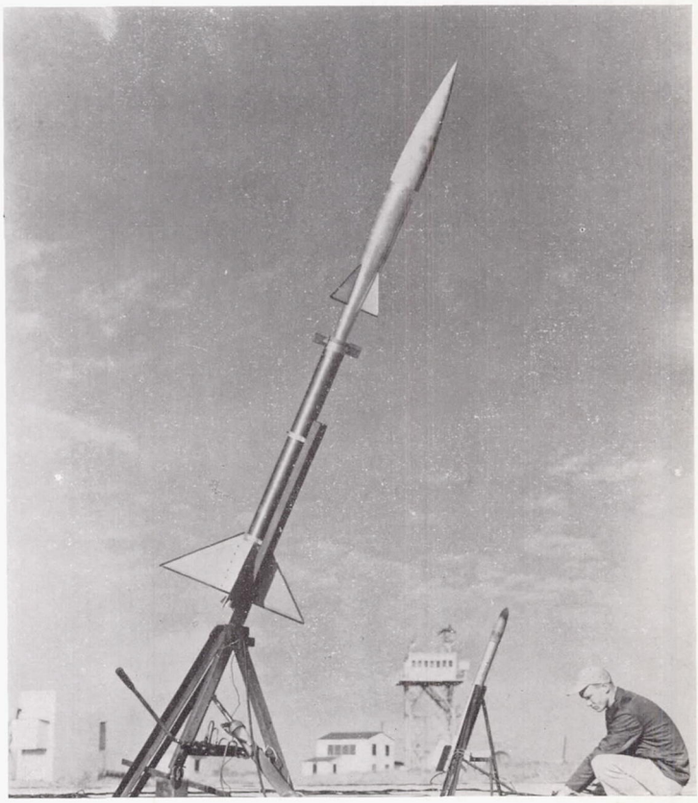

(b) Nonducted model A on the launcher. L–73803.1

FIGURE 5.—Concluded.

TABLE II.—PHYSICAL CHARACTERISTICS OF THE MODELS

Designation	Forebody profile	Forebody fineness ratio	External lip angle, deg	Inlet contraction ratios tested for configurations—		
				1	2	3
Cowling I	NACA 1–49–300	3. 0	90	1. 0	0. 83	0. 67
Cowling II	Parabolic	3. 0	9. 8	1. 0	. 83	. 67
Cowling III	Sharp lip conic, 4.9° half-angle	3. 0	4. 9	1. 0	. 83	. 67
Cowling IV	Beveled lip conic, 4.4° half-angle	3. 0	9. 8	1. 0	. 83	. 67
Cowling V	Blunt lip conic, 4.4° half-angle	3. 0	90	1. 0	. 83	. 67
Cowling VI	NACA 1–40–250	2. 5	90	1. 0	. 75	. 56
Nonducted model A	Parabolic	4. 2	------	---	---	---
Nonducted model B	Parabolic	3. 6	------	---	---	---

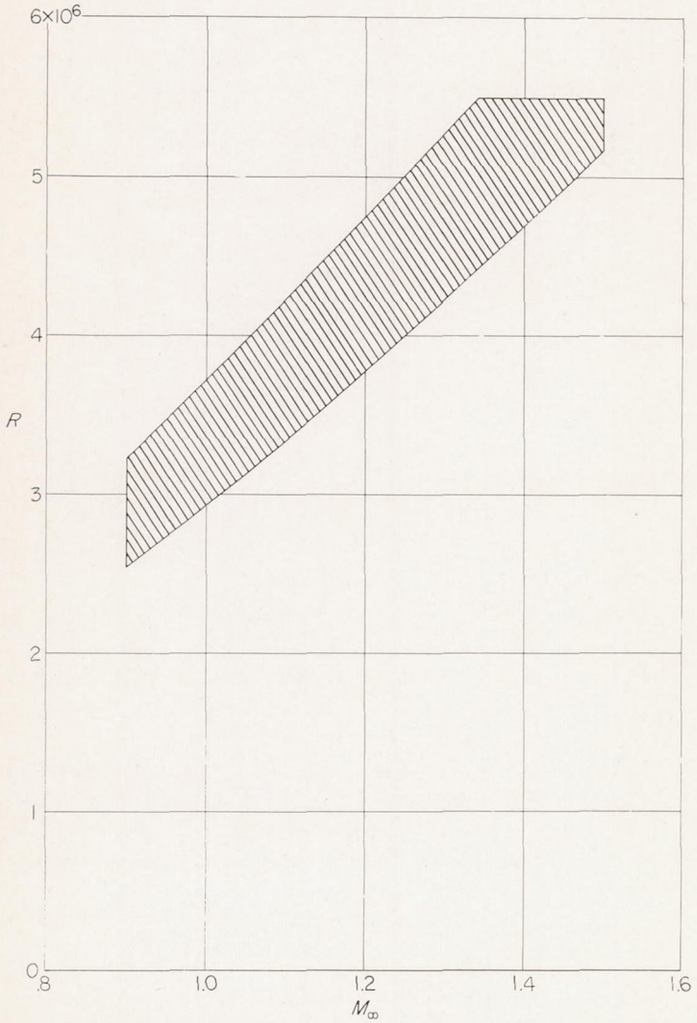

FIGURE 6.—Range of variation of Reynolds number, based on body maximum diameter, with Mach number for models tested.

In order to facilitate the building and flight testing of models of many different inlet contours, all but three of the models were built without telemeters. Total drag coefficients were obtained over the flight Mach number range from computations based on the CW Doppler radar velocity measurements, the flight path indicated by the NACA modified SCR 584 tracking radar, and radiosonde observations. Corrections were made for the horizontal component of the wind velocity and for flight-path curvature. A telemeter was used with a model (cowling II, configuration 3) to measure the static pressures at the inlet minimum-area station, the exit, and at two stations on the afterbody. Telemeter measurements were also made of three afterbody static pressures on a second model (cowling VI, configuration 3) and of the base pressure on nonducted model B.

The internal contour of the model was made so that at supersonic speeds the inlet was started or choking occurred at the minimum area just back of the inlet, while the exit was choked for all cases. The exit area of each ducted model was made equal to 1.05 times the inlet minimum area in order that the exit would stay choked to as low a free-stream Mach number as possible to permit evaluation of the internal drag. The duct was made cylindrical for at least 1.2 exit diameters ahead of the exit to aid in providing uniform static pressure at the exit. The fairly large contraction of at least 4 to 1 from near the maximum-diameter station to the exit assured sonic rather than supersonic exit velocities and also helped in providing uniform total pressure at the exit. The entering mass flow and the internal drag can, therefore, be calculated for the Mach number range over which these choking conditions existed. The method used for making these calculations is presented in the appendix.

Figure 7 compares the values of $C_{D,int}$ and m/m_∞ calculated as indicated in the appendix with the values computed from measurements made with a telemetered model (cowling II, configuration 3). The good agreement shown is believed to justify use of the calculated results at $M_\infty \geqq 0.9$, although at subsonic speeds some of the assumptions involved are not quite fulfilled.

ACCURACY OF DATA

The accuracy of the data is estimated to be within the following limits:

m/m_∞, for $M_\infty \geqq 1.0$	±0. 01
$C_{D,ext}$	±0. 01
C_p	±0. 015
M_∞	±0. 01

RESULTS AND DISCUSSION

EFFECT OF AFTERBODY LENGTH

Because the afterbody length was slightly greater for the models admitting lesser mass flow, it is necessary to examine the differences in $C_{D,ext}$ associated with differences in model length. Figure 8 presents measured afterbody pressure

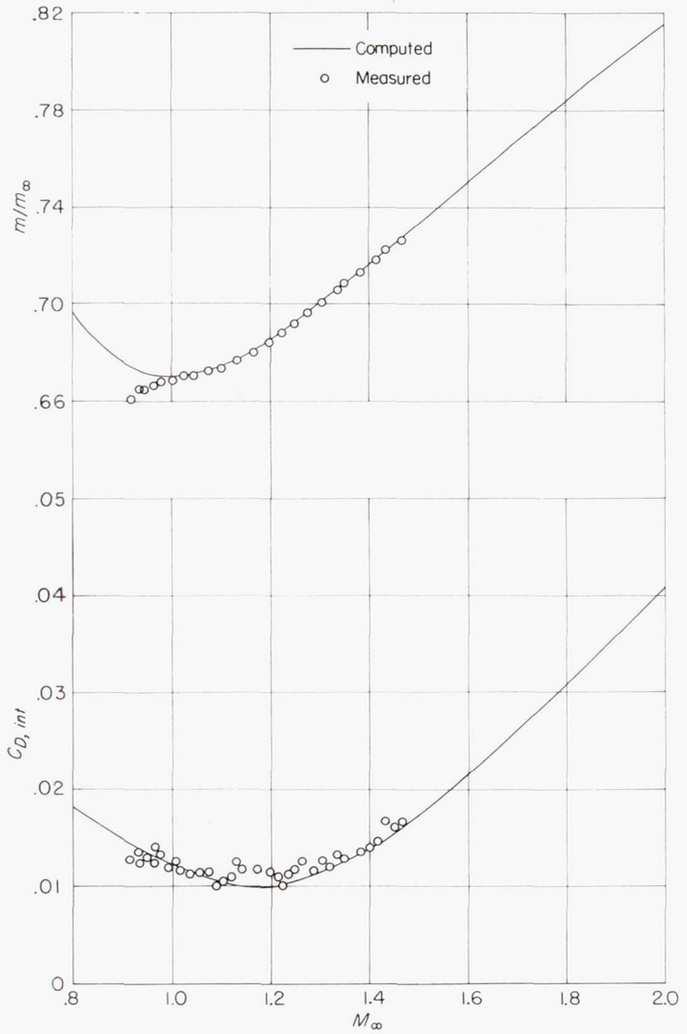

FIGURE 7.—Variation of internal drag coefficient and mass-flow ratio with Mach number for models with telemeter.

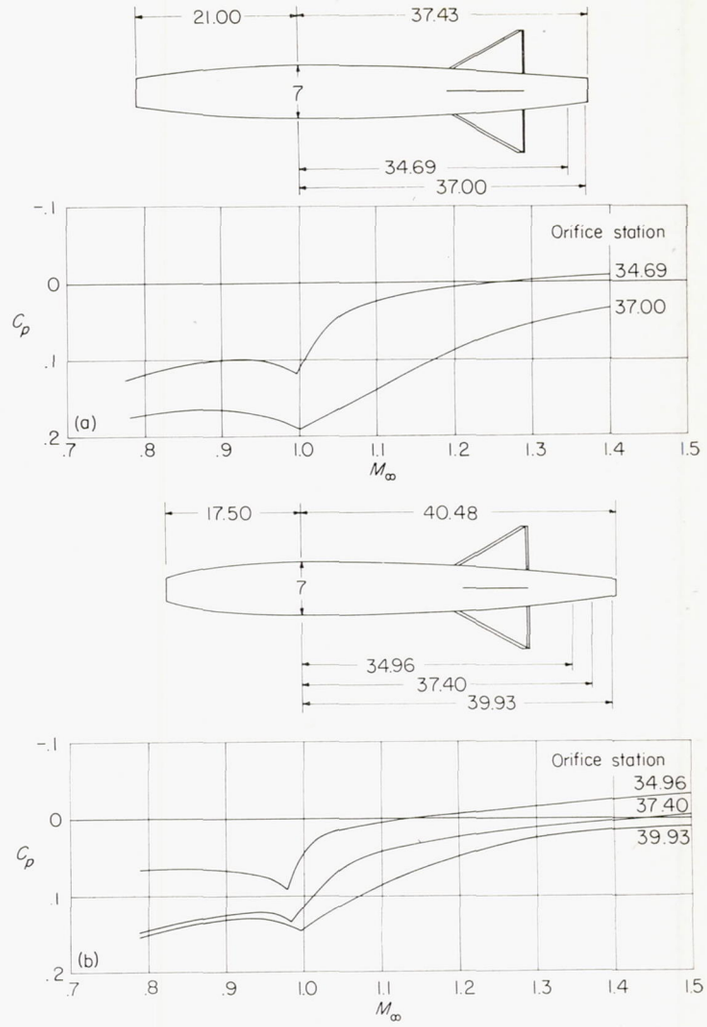

(a) Cowling II: parabolic; configuration 3.
(b) Cowling VI: NACA 1–40–250; configuration 3.

FIGURE 8.—Variation of pressure coefficient with Mach number at several afterbody stations for two ducted models. All dimensions are in inches.

coefficients for two ducted models as a function of Mach number. The static-pressure orifices were located at the body stations on a longitudinal line that passed midway between two fins (see fig. 8).

The data of reference 3 indicate that large changes in nose shape have negligible effect on the pressures over the rearward portion of the body length. It is, therefore, assumed that the differences in C_p shown in figure 8 are caused primarily by the differences in afterbody length and by the effects of the exit and of the jet propagating upstream through the boundary layer at supersonic Mach numbers or through the subsonic flow field at the exit in the lower range of test Mach numbers.

Integration of the measured pressures to obtain a pressure drag coefficient for the portion of each model rearward of station 34 (where both models had nearly the same pressure coefficient) gave the same value for each model, within $\Delta C_D = 0.001$. The coefficient of skin-friction drag acting on the incremental surface area of the longer afterbody is estimated to be 0.002. Any differences in $C_{D,ext}$ caused by varying the length of the afterbody, therefore, are believed to be small and well within the accuracy of $C_{D,ext}$.

BASIC DATA

The curves of external drag for each ducted model are presented in figure 9. The mass-flow ratio associated with each drag curve is also given. For configuration 1 with each cowling the mass-flow ratio was unity at all Mach numbers; that is, no air was spilled. An increasing amount of air was spilled with configurations 2 and 3. The inlet-contraction ratios of configurations 2 and 3 were too great to permit the inlets to start in the test Mach number range.

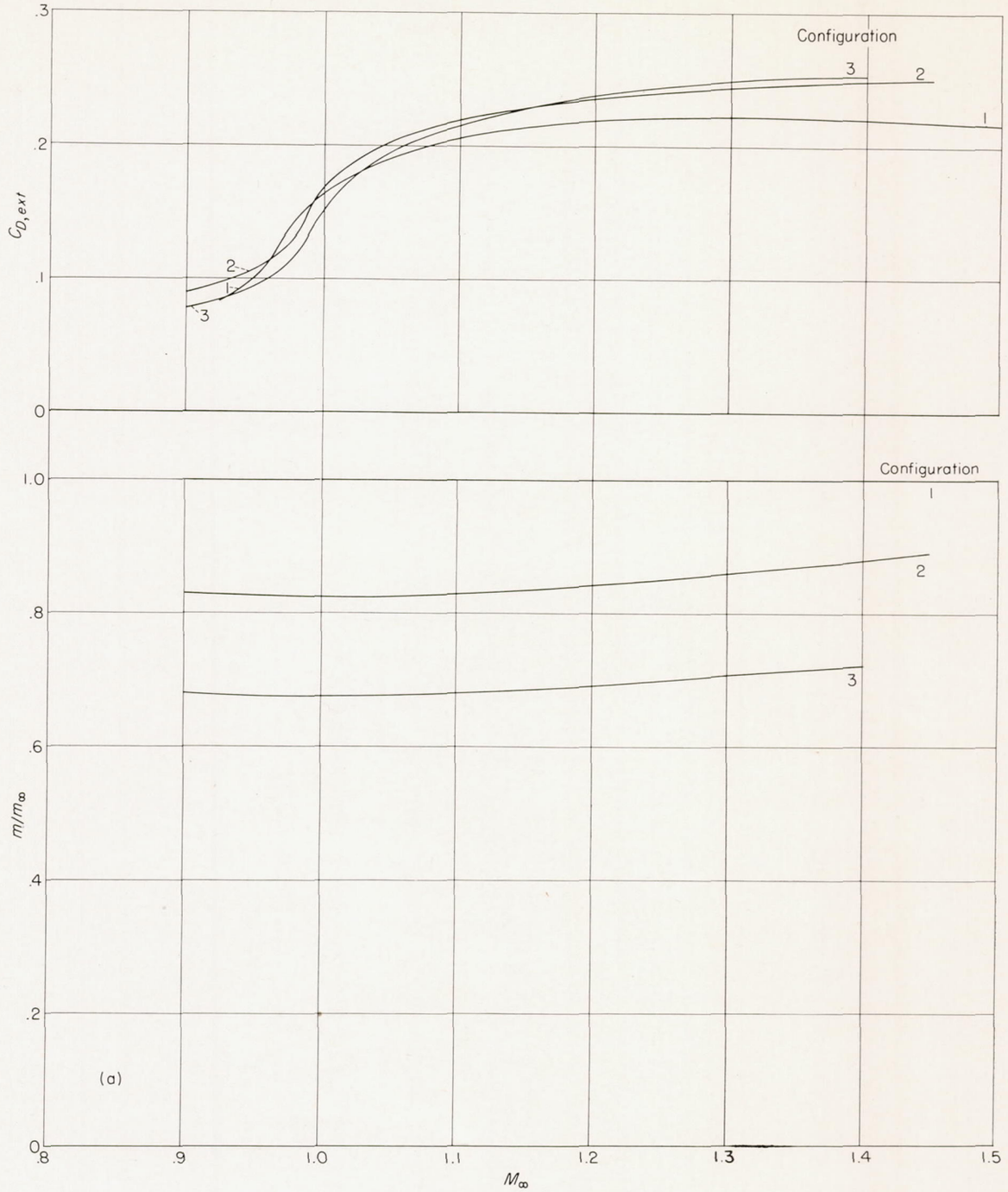

(a) Cowling I: NACA 1–49–300.

FIGURE 9.—Variation of external drag coefficient and mass-flow ratio with Mach number for the models with various cowling shapes.

391987—56——2

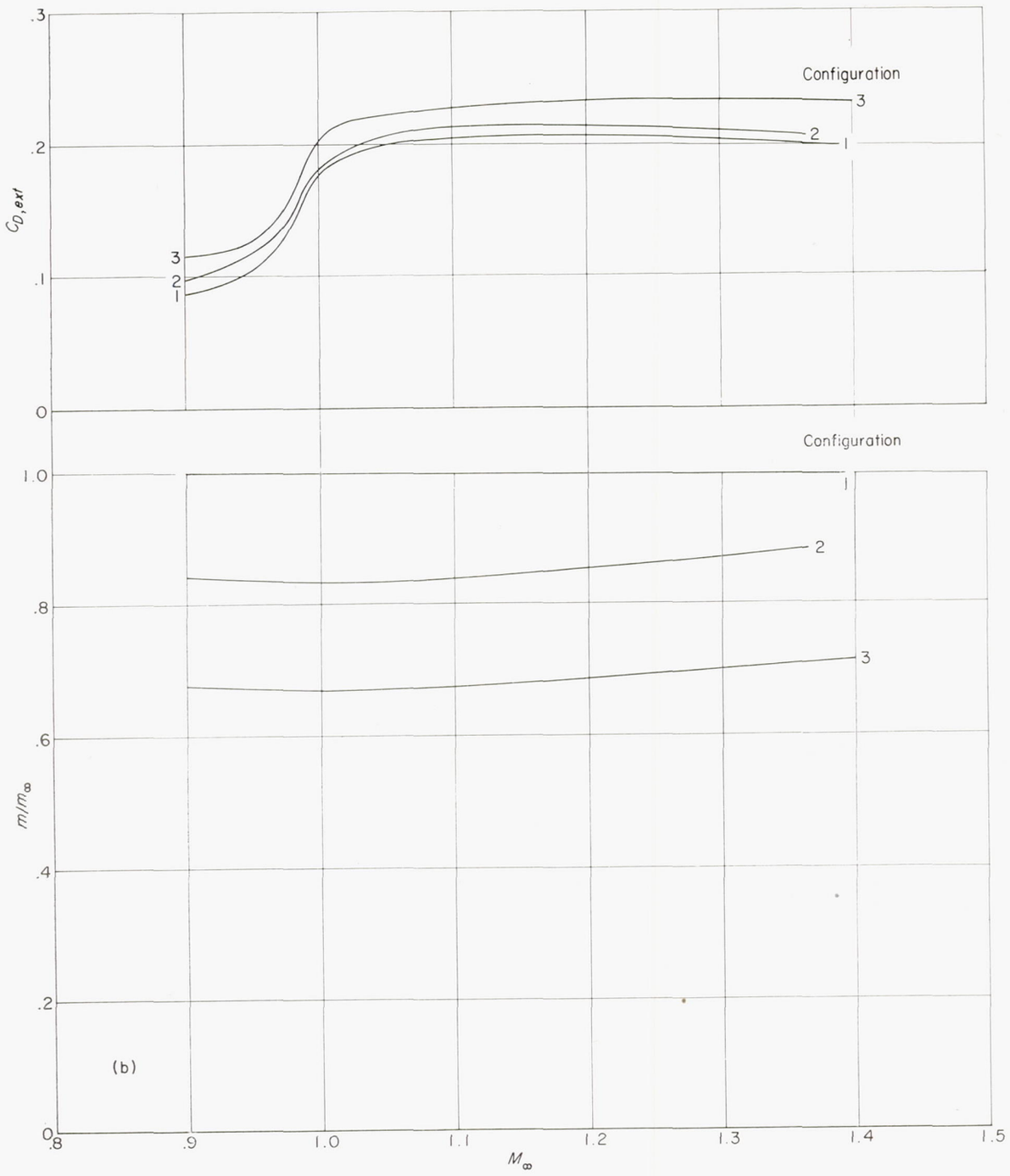

(b) Cowling II: parabolic.

FIGURE 9.—Continued.

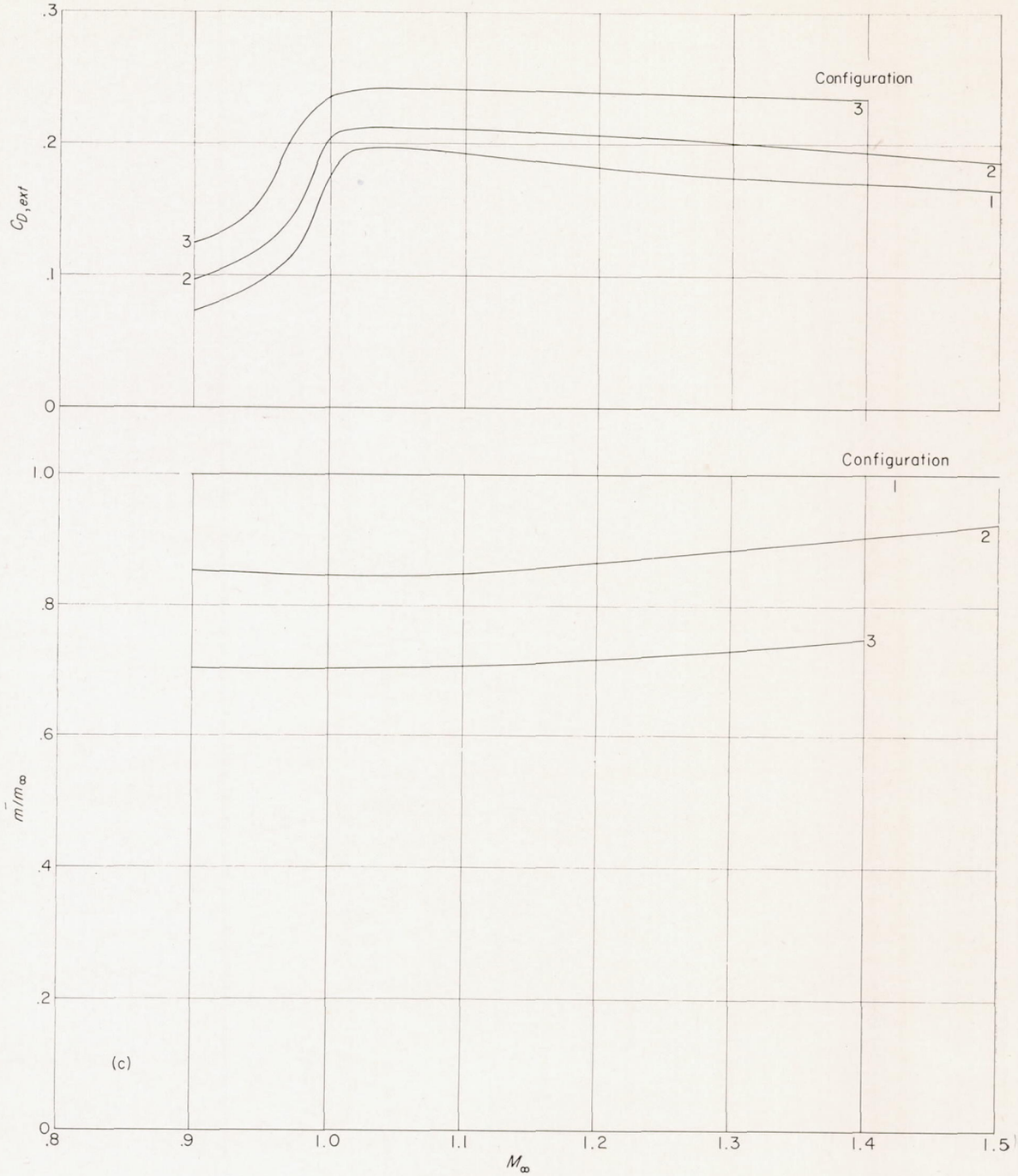

(c) Cowling III: conic, sharp lip.

FIGURE 9.—Continued.

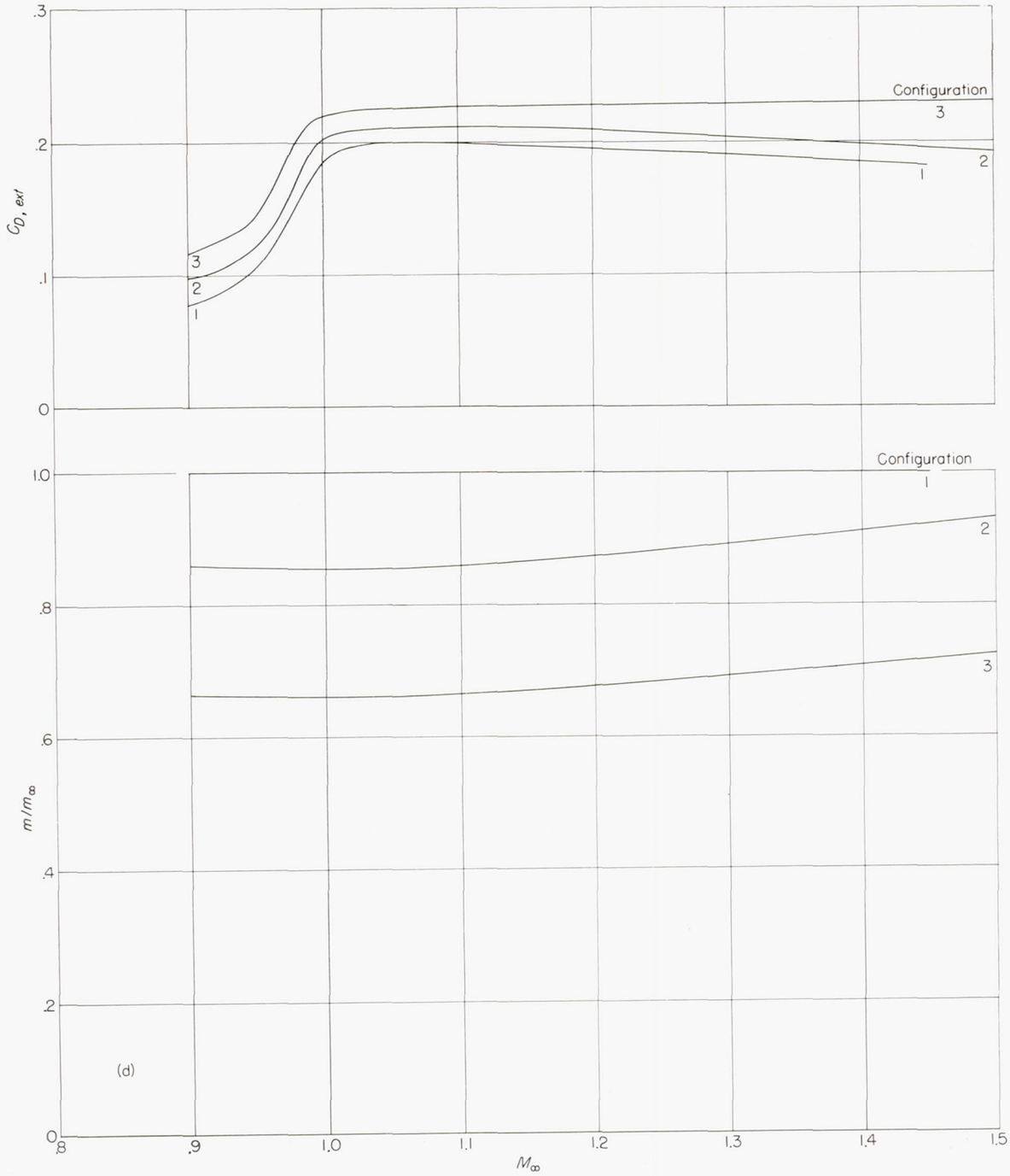

(d) Cowling IV: conic, beveled lip.

FIGURE 9.—Continued.

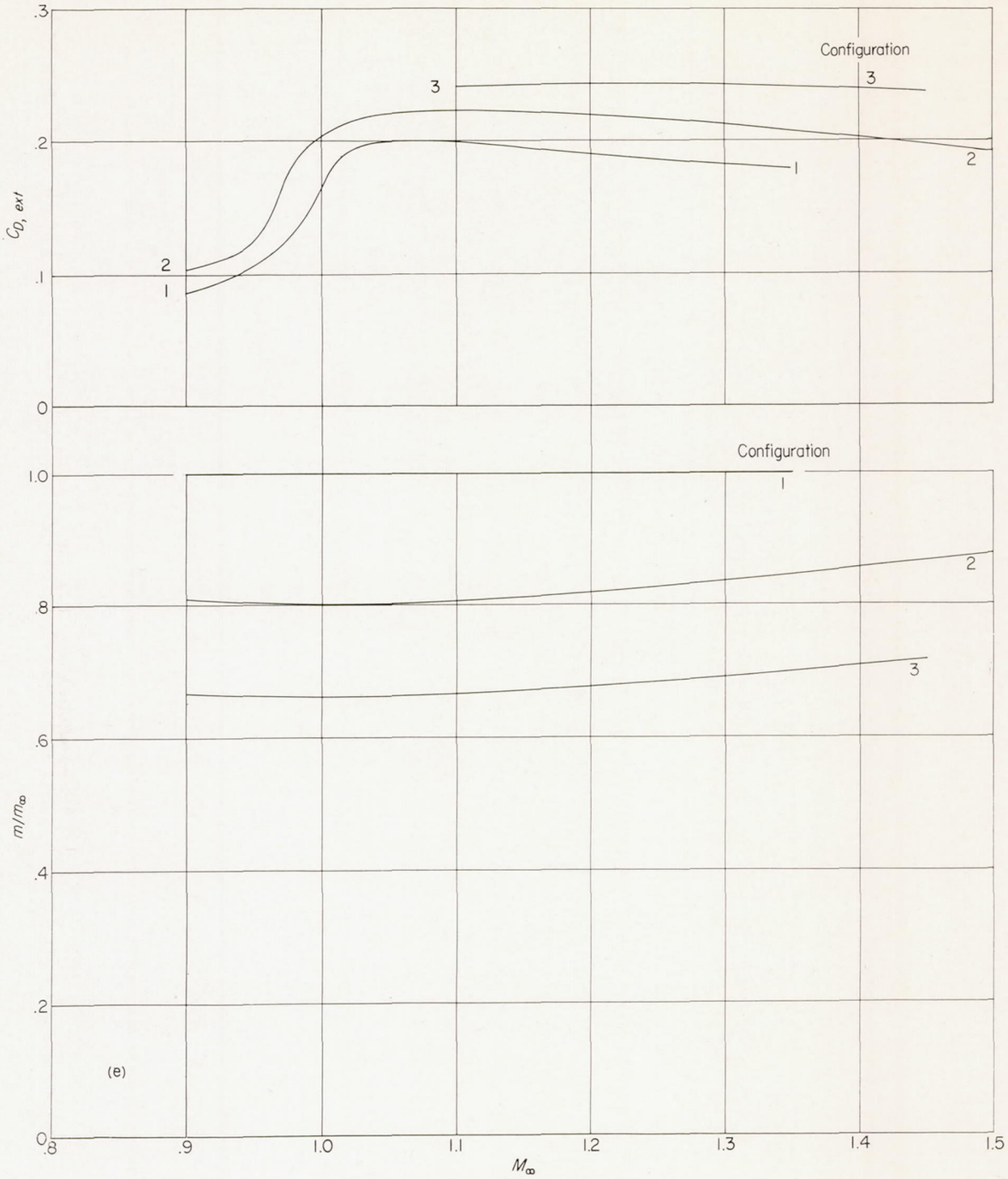

(e) Cowling V: conic, blunt lip.

FIGURE 9.—Continued.

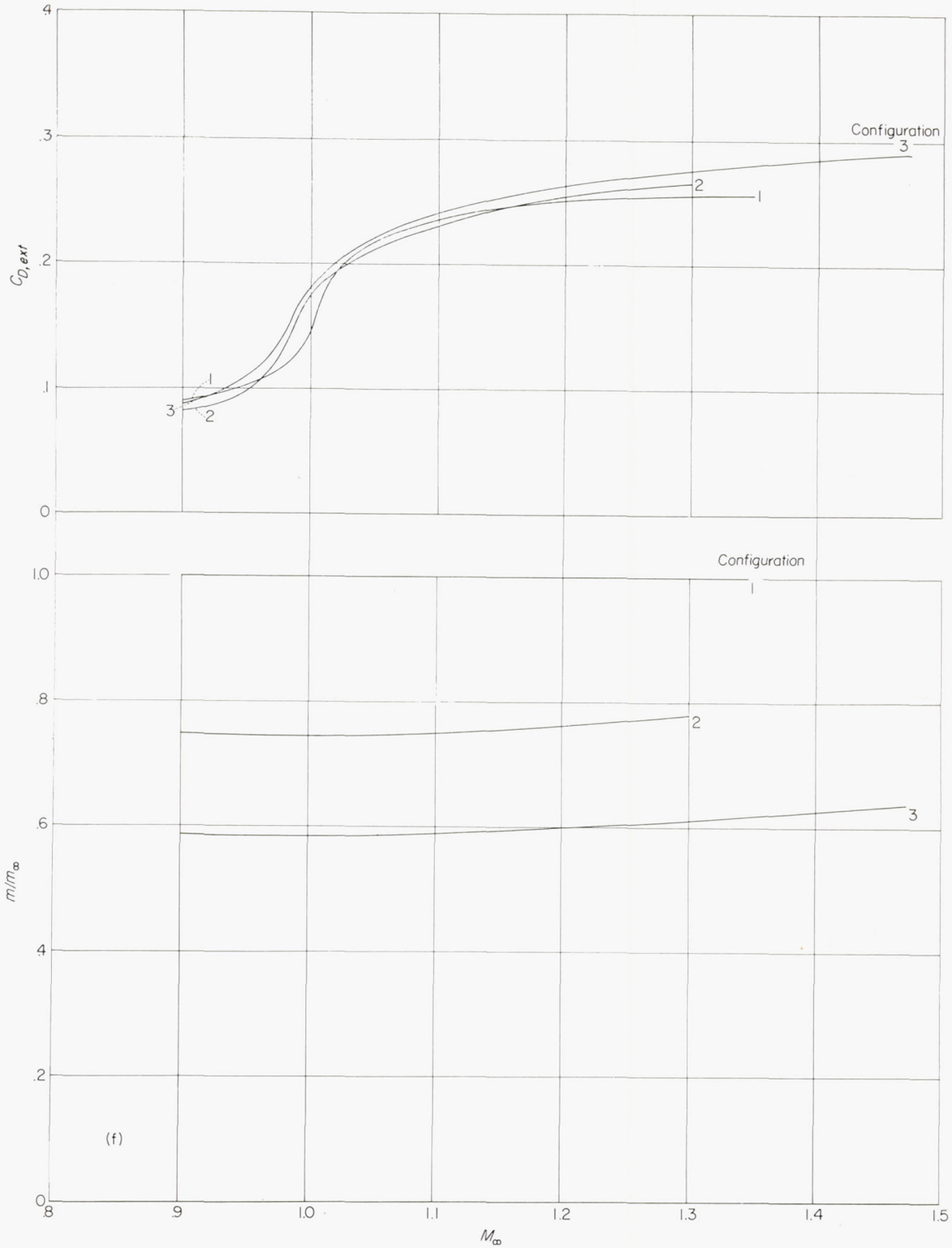

(f) Cowling VI: NACA 1-40-250.

FIGURE 9.—Concluded.

The curves of total drag coefficient as a function of Mach number are given in figure 10 for the two nonducted models. Base drag coefficient was measured for nonducted model B only and is also shown in figure 10.

EFFECT OF COWLING SHAPE

The drag-coefficient curves at $m/m_\infty=1.0$ for the various normal-shock inlet models with cowlings of fineness ratio 3.0 are shown superimposed in figure 11 for comparison purposes. Also shown is the curve for the total-minus-base drag coefficient for solid body model A. The base drag coefficient of model A was obtained by using the measured base pressure coefficient of model B.

Inspection of figure 11 indicates that in the transonic range below $M_\infty \approx 1.1$ all the ducted models with cowlings of fineness ratio 3.0 have about the same drag coefficient. As the Mach number increases the curves diverge; the sharp-lip conic cowling has the least drag and the NACA 1-series cowling has the greatest drag. Comparison of the drag of the three conic cowling models at $M_\infty > 1.2$ indicates that, for these cowlings of constant fineness ratio, beveling or blunting the lip caused a small increase in drag over that of the sharp-lip conic cowling. It should be noted, however, that, of the two conic cowlings which were identical except for lip shape (cowlings IV and V), the blunt-lip conic cowling had slightly lower drag than the beveled-lip conic cowling. Thus, it appears that the effect of lip bluntness on drag is critically dependent on the manner of blunting the lip. Because the NACA 1-series cowling and the blunt-lip conic cowling had the same external lines in the region of the inlet lip, it is apparent that the higher drag of the NACA 1-series cowling is associated with its greater fullness farther rearward.

The drag of the pointed nonducted body is greater than the external drag of all the inlet models in the transonic range and at $M_\infty > 1.2$ is about equal to that of the cowling which was defined by the same parabolic arc. At all test Mach numbers greater than 1.05, the external drag of the conic-cowling models was less than drag of the solid body for mass-flow ratios greater than 0.9. The data of reference 4 indicate that the solid body is a low-drag configuration at supersonic speeds. The lower drags obtained with the conic cowlings indicate therefore that these also must be considered as low-drag configurations.

The variation of external drag coefficient with mass-flow ratio at $M_\infty=1.3$ is shown for the various cowlings in figure 12 by cross plotting the data of figure 9. The increase in drag with spillage is different for each cowling and is greatest for the conic cowling with sharp lips and least for the NACA 1-series cowling I. At $m/m_\infty=0.8$, the three conic cowlings and the parabolic cowling all have about the same drag. The NACA 1-series cowling has the greatest drag at all flow rates tested because of its high drag at maximum-flow rate.

The rate of increase of drag coefficient with spillage for the various cowlings is better compared in figure 13 where the slopes of the curves of figure 12 and similar ones for other Mach numbers are shown for each cowling. The slope of the additive drag curve computed by assuming one-dimensional flow is also shown as a function of Mach number. The departure of the curves of figure 13 from the additive drag curve is caused by the reductions in cowling pressure drag with spillage. The data indicate very little change in cowling pressure drag with spillage for the sharp-lip inlet and large reductions for the NACA 1-series inlet. This trend is consistent with previous experiences with leading-edge suction for wings at angle of attack. Cowling pressure distributions at several flow rates are shown in reference 3 for NACA 1-series cowlings.

NACA 1-40-250 COWLING

The models with the NACA 1–40–250 cowling and the related nonducted body B were tested for purpose of comparison of results with those results reported in reference 1. These models and those of reference 1 differed only in fin geometry and overall length. The flight-test technique for obtaining the data was considerably different from that reported herein. Comparison of the data of figures 9(f) and 10 with those presented in reference 1 indicates that, when allowance is made for the differences in fin drag, the measured drag coefficients of the present tests are essentially the same as those of reference 1 for both the ducted and nonducted models. A comparison of the results for the ducted models is shown in figure 14 for several Mach numbers. The solid curve is the external drag coefficient, as presented in reference 1, which was extrapolated to $m/m_\infty=1.0$. The points are the measured values obtained for cowling VI of this investigation. The long dashed curve was obtained by correcting the data of reference 1 for the difference in fin-plus-interference drag. The difference in fin-plus-interference drag was obtained by subtracting the total-minus-base drag of nonducted model B from the total-minus-base drag of the solid body of reference 1.

Comparison of the minimum drag of the NACA 1–40–250 nose-inlet model with the minimum drag of the NACA 1–49–300 model (cowling I) shows that the subsonic drags were essentially the same, but, for $M_\infty > 1.02$, the shorter, blunter, NACA 1–40–250 cowling had the higher drag.

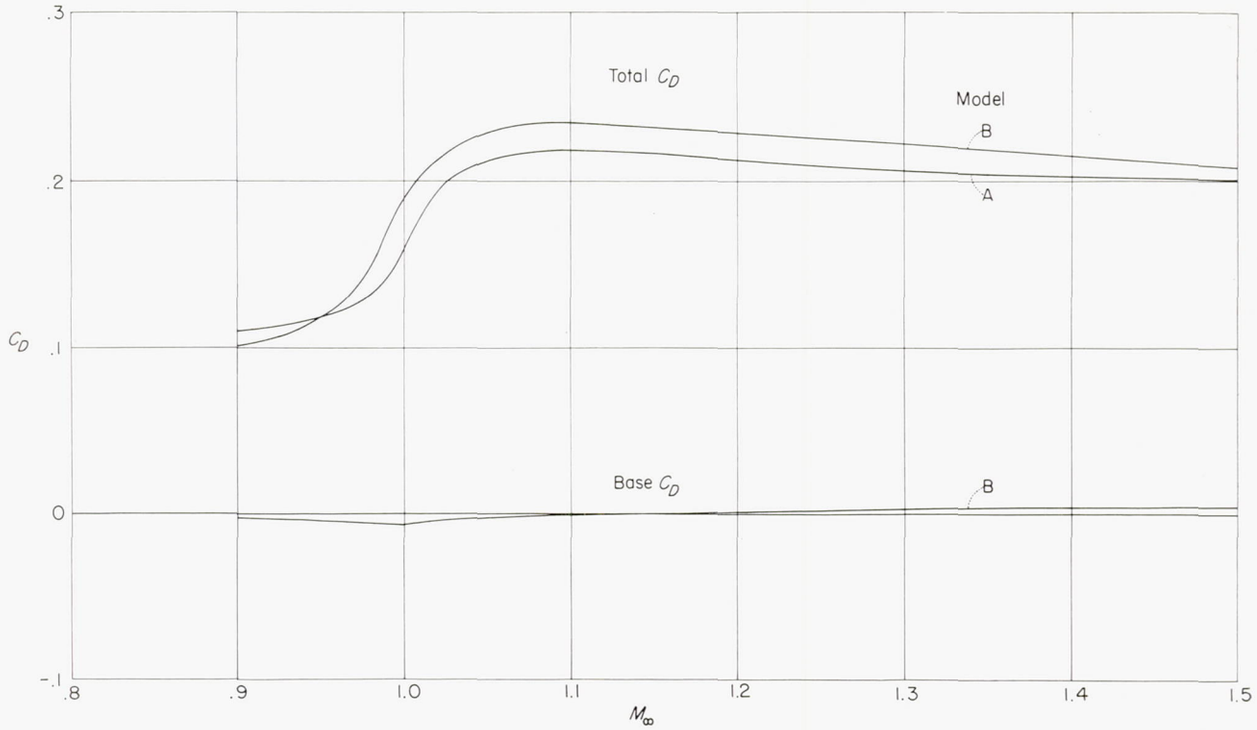

FIGURE 10.—Variation of total and base drag coefficients with Mach number for the nonducted models.

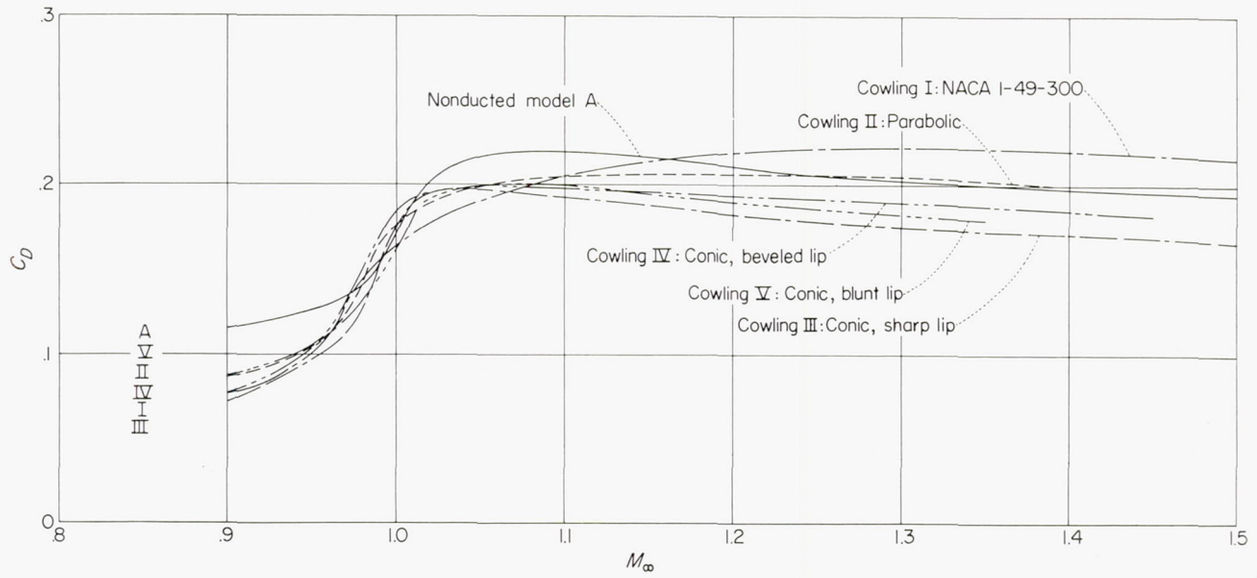

FIGURE 11.—Variation with Mach number of external drag coefficient for ducted models with various cowlings of fineness ratio 3.0 and total minus base drag coefficient for nonducted model A. $\frac{m}{m_\infty}=1.0$.

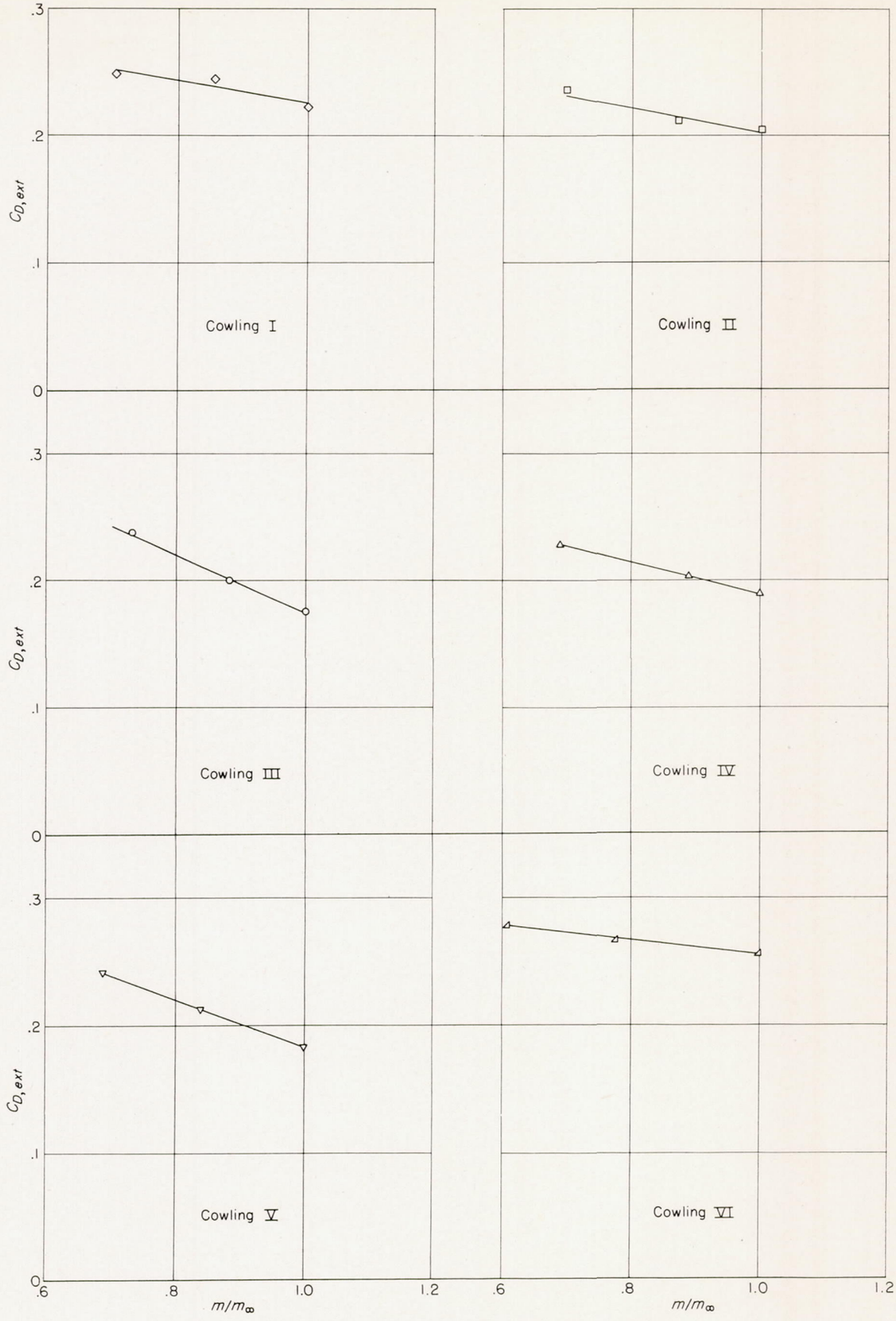

FIGURE 12.—Variation of external drag coefficient with mass-flow ratio at $M_\infty = 1.3$.

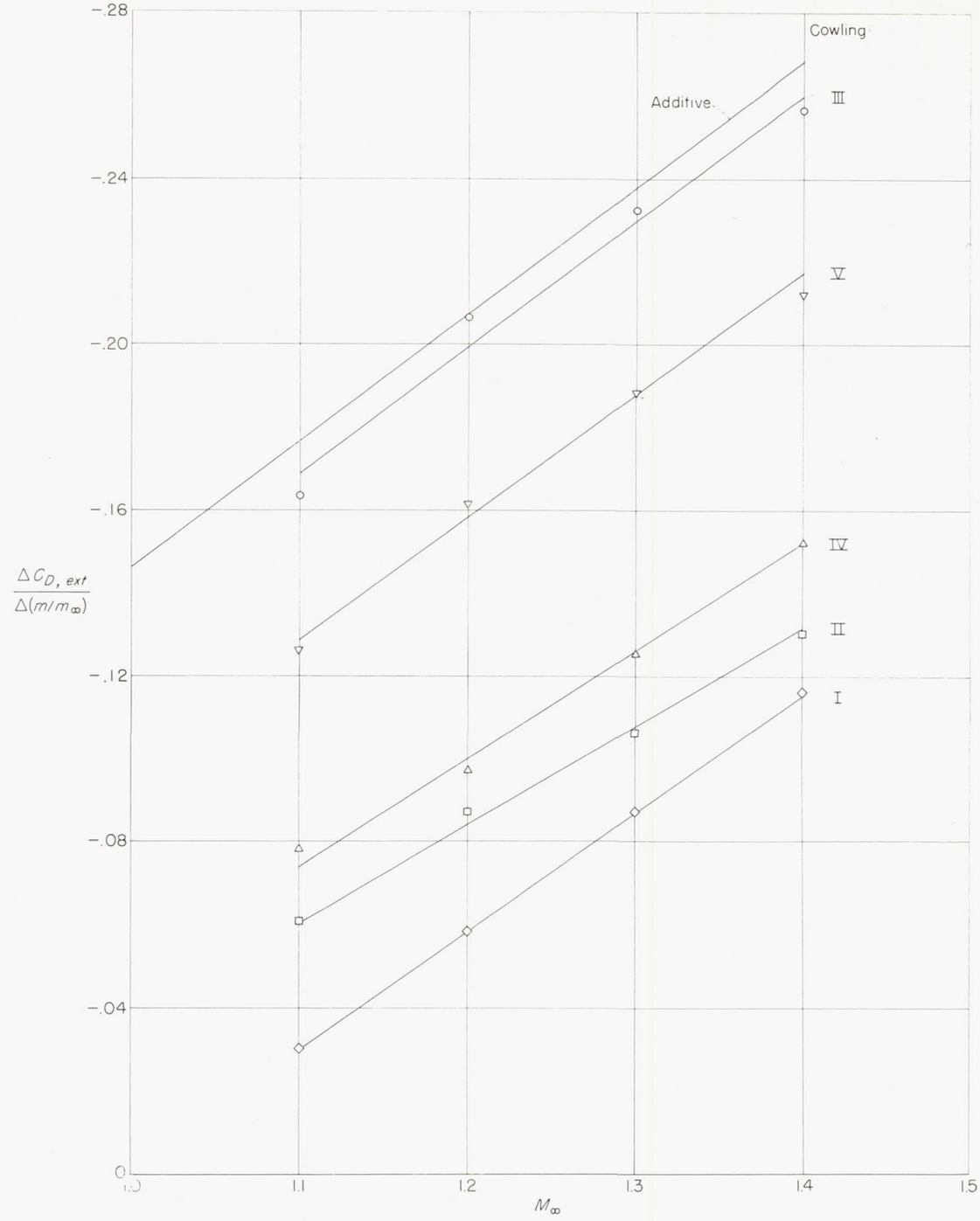

FIGURE 13.—Variation with Mach number of the change in external drag coefficient with change in mass-flow ratio for models with various cowlings of fineness ratio 3.0.

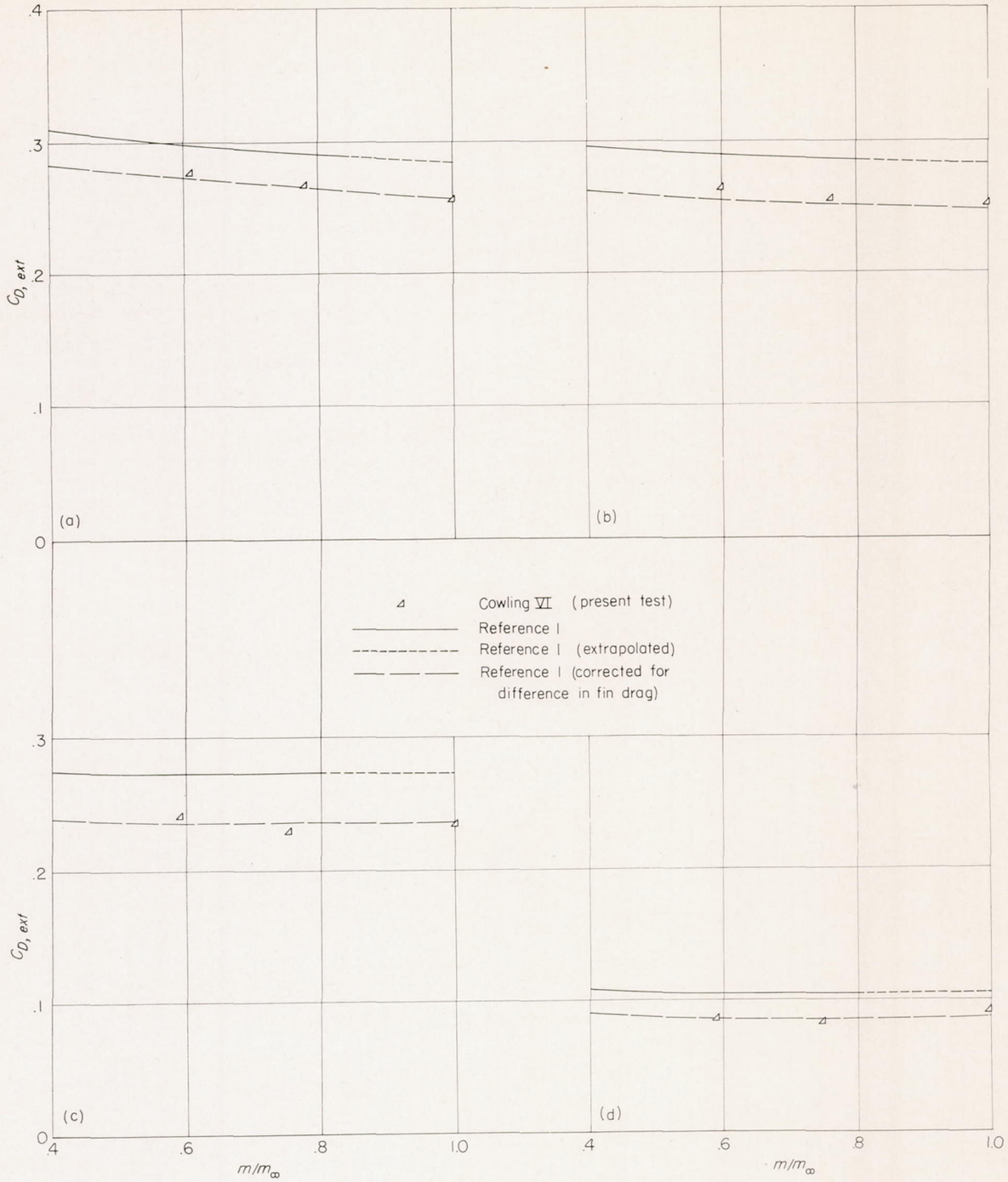

(a) $M_\infty = 1.3$. (b) $M_\infty = 1.2$.

(c) $M_\infty = 1.1$. (d) $M_\infty = 0.9$.

FIGURE 14.—Comparison of the external drag coefficient of cowling VI (NACA 1–40–250) with reference 1 at various Mach numbers.

CONCLUSIONS

Models having normal-shock nose inlets with NACA 1-series, parabolic, and conic cowlings have been tested at free-stream Mach numbers from 0.9 to 1.5 and flow ratio from 0.7 to 1.0 at an angle of attack of 0°. Two related nonducted bodies were also tested for comparison purposes. Within the range of the tests, the following conclusions apply:

1. At the maximum flow rate, the conic, parabolic, and NACA 1-series cowlings all had about the same external drag at a Mach number of approximately 1.1. At higher Mach numbers, the drag of the conic cowling was appreciably less than that of the parabolic or NACA 1-series cowlings.

2. Blunting or beveling the lip of the conic cowling while keeping the cowling fineness ratio constant resulted in drag coefficients slightly higher than for the sharp-lip conic cowling at maximum flow rate. At a mass-flow ratio of about 0.8, the conic cowlings with sharp, blunt, or beveled lips and the parabolic cowling all give about the same drag. The higher drag of the NACA 1–49–300 cowling compared with the blunt-lip conic cowling is associated with its greater fullness back of the inlet.

3. The sharp-lip conic cowling experienced only small reductions in cowling pressure drag with air spillage, whereas the NACA 1-series cowling had large reductions. Because of its high drag at maximum flow rate, however, the NACA 1-series cowling gave the greatest drag at all flow rates of all the cowlings tested at Mach numbers greater than 1.1.

4. The drag of the conic-cowling models at high mass-flow rates was less than that of a related parabolic nonducted model at Mach number greater than 1.05. At Mach number greater than 1.2, the drag of the parabolic-cowling model was about the same as that of the nonducted model.

LANGLEY AERONAUTICAL LABORATORY,
NATIONAL ADVISORY COMMITTEE FOR AERONAUTICS,
LANGLEY FIELD, VA., *September 8, 1953.*

APPENDIX

METHOD USED TO DETERMINE THE DRAG AND MASS-FLOW RATIO FOR NORMAL-SHOCK NOSE INLETS

The total drag was obtained from the CW Doppler radar and the SCR 584 tracking radar measurements of velocity and flight path, respectively. Thus,

$$D_t=-W\left(\frac{1}{g}\frac{dV}{dt}+\sin\theta\right) \tag{A1}$$

The external drag is defined, in the usual manner, as the sum of the dragwise component of the aerodynamic pressure and viscous forces acting on the external surface of the body plus the dragwise component of the aerodynamic pressure forces acting on the external contour of the entering streamline. Thus, the external drag is obtained by subtracting the internal drag from the total drag:

$$D_{ext}=D_t-D_{int} \tag{A2}$$

The internal drag is obtained from the following equation by applying the momentum equation between the free stream ahead of the inlet and the duct exit:

$$D_{int}=\gamma p_\infty M_\infty{}^2A_\infty-\gamma p_eM_e{}^2A_e-(p_e-p_\infty)A_e \tag{A3}$$

where the unknowns M_e, p_e, and A_∞ are obtained in the following manner. Since the exit is assumed to be choked (i. e., $M_e=1.0$),

$$p_e=0.528p_{t,\infty}\frac{A_\infty}{A_e}\left(\frac{A_{cr}}{A}\right)_\infty \tag{A4}$$

where M_∞ is less than M_∞ necessary to start the inlet, if it is assumed that $M_1=1.0$ and $p_{t,1}=p_t{}'_{,\infty}$,

$$A_\infty=\frac{p_t{}'_{,\infty}/p_{t,\infty}}{(A_{cr}/A)_\infty}A_1 \tag{A5a}$$

and where M_∞ is equal to or greater than M_∞ necessary to start the inlet,

$$A_\infty=A_i \tag{A5b}$$

The mass-flow ratio is

$$m/m_\infty=\frac{\rho_\infty A_\infty V_\infty}{\rho_\infty A_iV_\infty}=\frac{A_\infty}{A_i} \tag{A6}$$

Obviously the mass flow and internal drag can be properly evaluated in the manner indicated only for the range of M_∞ for which the flow follows the assumed pattern. The minimum Mach number for which the inlet and exit will be choked depends on the relative size of the minimum area at the inlet and exit and on the internal losses. The models of the present investigations were designed to choke at both the inlet and exit at Mach numbers from slightly above sonic to the maximum attained.

One ducted model with pressure instrumentation and telemeter was flight tested in order to determine the minimum Mach number at which the assumed choking conditions existed at the inlet and exit. The measured inlet and exit static pressures together with the pitot stagnation pressure at the inlet were used to evaluate the internal drag and mass flow for this model. The method of reducing these data was the same as that discussed in reference 1 for ducted-nose-inlet models with telemeters.

The pressure measurements indicated that the inlet and exit were choked for values of M_∞ greater than 1.03 and 1.08, respectively. The data of figure 7, however, show that the mass flow and internal drag computed according to equations (A3) to (A6) is in excellent agreement with the measured values at all supersonic Mach numbers. At $M_\infty=0.9$ the computed $C_{D,int}$ is still in good agreement with the measured value and the computed m/m_∞ is about 0.015 greater than that measured. It is, therefore, believed that the method of calculation gives the correct values of $C_{D,int}$ and m/m_∞ at $M_\infty>1.03$. For Mach numbers from 0.9 to 1.03, a small error is introduced in the magnitude of m/m_∞ only.

REFERENCES

1. Sears, R. I., and Merlet, C. F.: Flight Determination of the Drag and Pressure Recovery of an NACA 1–40–250 Nose Inlet at Mach Numbers From 0.9 to 1.8. NACA TN 3218, 1955. (Supersedes NACA RM L50L18.)
2. Baals, Donald D., Smith, Norman F., and Wright, John B.: The Development and Application of High-Critical-Speed Nose Inlets. NACA Rep. 920, 1948. (Supersedes NACA ACR L5F30a.)
3. Pendley, Robert E., and Robinson, Harold L.: An Investigation of Several NACA 1-Series Nose Inlets With and Without Protruding Central Bodies at High-Subsonic Mach Numbers and at a Mach Number of 1.2. NACA TN 3436, 1955. (Supersedes NACA RM L9L23a.)
4. Hart, Roger G., and Katz, Ellis R.: Flight Investigations at High-Subsonic, Transonic, and Supersonic Speeds to Determine Zero-Lift Drag of Fin-Stabilized Bodies of Revolution Having Fineness Ratios of 12.5, 8.91, and 6.04 and Varying Positions of Maximum Diameter. NACA RM L9I30, 1949.

U. S. GOVERNMENT PRINTING OFFICE: 1957